EARTHQUAKES

Stress drops of induced and tectonic earthquakes in the central United States are indistinguishable

Yihe Huang,[1]* William L. Ellsworth,[2] Gregory C. Beroza[2]

Copyright © 2017 The Authors, some rights reserved; exclusive licensee American Association for the Advancement of Science. No claim to original U.S. Government Works. Distributed under a Creative Commons Attribution NonCommercial License 4.0 (CC BY-NC).

Induced earthquakes currently pose a significant hazard in the central United States, but there is considerable uncertainty about the severity of their ground motions. We measure stress drops of 39 moderate-magnitude induced and tectonic earthquakes in the central United States and eastern North America. Induced earthquakes, more than half of which are shallower than 5 km, show a comparable median stress drop to tectonic earthquakes in the central United States that are dominantly strike-slip but a lower median stress drop than that of tectonic earthquakes in the eastern North America that are dominantly reverse-faulting. This suggests that ground motion prediction equations developed for tectonic earthquakes can be applied to induced earthquakes if the effects of depth and faulting style are properly considered. Our observation leads to the notion that, similar to tectonic earthquakes, induced earthquakes are driven by tectonic stresses.

INTRODUCTION

Quantifying ground motion hazard from earthquakes triggered by fluid injection related to unconventional hydrocarbon development (*1*) is an important aspect of managing the risk that they pose. A key question is whether induced earthquakes excite ground motion differently than tectonic earthquakes. Stress drop, the difference in shear stress on a fault before and after an earthquake, can exert a strong influence on ground motions for frequencies of engineering concern (*2*, *3*). Hough (*4*, *5*) infers that induced earthquakes have lower stress drops than tectonic earthquakes based on a comparison of noninstrumental "Did You Feel It?" intensities. Other studies (*6*–*8*) find that induced earthquake sequences in Arkansas and Western Canada have comparable stress drops to tectonic earthquakes. Moreover, instrumental intensities recorded for induced earthquakes in Oklahoma, Texas, and Kansas at distances less than 10 km, wherein "Did You Feel It?" data are sparse, are consistent with the predicted ground motions of tectonic earthquakes (Fig. 1) (*9*). Here, we use available instrumental recordings to estimate stress drops of earthquakes across the central United States and eastern North America. We find that, once faulting mechanism and depth are accounted for, stress drops of induced and tectonic earthquakes are indistinguishable. This is consistent with the hypothesis that, similar to tectonic earthquakes, induced earthquakes are driven by tectonic stresses, with their time of occurrence advanced by fluid injection.

RESULTS

We measure stress drops of induced and tectonic earthquakes with a moment magnitude (M_w) of 3.3 to 5.8 in the central United States and eastern North America that comprise three populations (Fig. 2). The first are central U.S. tectonic earthquakes in and around the New Madrid Seismic Zone and Wabash Valley Seismic Zone. The second are eastern U.S. and Canadian tectonic earthquakes located around and east of the Appalachians. The third are suspected induced earthquakes located to the west of these populations but to the east of the Rocky Mountains. For each population, we use small nearby earthquakes as empirical Green's functions (eGfs) to account for propagation and site effects in the interpretation of the spectra of larger earthquakes (*10*–*13*). The eGf approach does not require assumptions about the frequency dependence of attenuation nor the modeling of complex elastic wave propagation effects, resulting in accurate stress drop estimates (*14*, *15*).

For each earthquake, we use nearby events that are more than 1 magnitude unit smaller as eGfs. We focus on the *S*-wave spectral ratio (that is, the spectral ratio of the *S* wave of the master event to the *S* wave of the eGf) because it is better resolved than the *P*-wave spectral ratio as *S* waves have larger signal-to-noise ratios at available stations. We use five windows, overlapped by half the window duration, following the direct *S* wave to stabilize the spectral estimates (*16*). The window length is determined from the fit of the data (tables S2 to S4). We first stack *S*-wave spectral ratios over available stations and average the east and north components. We then solve for corner frequencies from the stacked spectral ratios using trust region reflective optimization (*7*). We repeat this process of calculating and stacking spectral ratios until we find a window length that minimizes the misfit between the stacked spectral ratio and the Brune spectral model (*17*). Figures S1 to S3 show the observed *S*-wave spectral ratios of the three populations of earthquakes. We calculate stress drops from seismic moments and corner frequencies using a circular crack model (*18*) and Brune's model parameters (*17*). A single shear wave velocity of 3.3 km/s is assumed for comparison purposes (Materials and Methods). The circular crack model is widely used in stress drop calculation and is a simple model for characterizing source effects on ground motion; however, earthquakes may have complex rupture processes with multiple subevents that cannot be modeled accurately as a circular crack. We discuss the assumption of a circular crack model when comparing our results with other stress drop studies, including finite fault models. We choose the Brune stress drop over alternatives to facilitate comparisons with the stress parameter used in the source term for ground motion prediction. Other spectral models (*19*) and source parameters (*20*, *21*) will lead to a systematic difference in stress drop estimates but with minimal influence on the relative stress drop values (*7*). We also bootstrap the misfits between the best-fit model and the stacked spectral ratios at each frequency interval and create synthetic spectral ratios by adding the resampled misfits to the stacked spectral ratios. The synthetic spectral ratios yield corner frequency estimates that appear as a Gaussian distribution. The possible range of stress drops are then derived from corner frequency estimates at the 95% confidence level (Materials and Methods).

We observe that the 22 induced earthquakes in the central United States have stress drops between 0.6 and 84 MPa with a median of

[1]Department of Earth and Environmental Sciences, University of Michigan, Ann Arbor, MI 48109, USA. [2]Department of Geophysics, Stanford University, Stanford, CA 94305, USA.
*Corresponding author. Email: yiheh@umich.edu

Downloaded from http://advances.sciencemag.org/ on September 24, 2020

5.3 MPa (Fig. 3). In comparison, the nine tectonic earthquakes in the central United States have stress drops between 4.6 and 30 MPa with a median of 8.4 MPa. The observed range of stress drop estimates may be influenced by a number of factors, including variability in source geometry, rupture speed, local wave velocities (*22*), and uncertainty in the corner frequency. Another contributing factor to the observed stress drop variability is earthquake depth, which may have large uncertainty. We compile the possible depth range for each earthquake from a variety of data sets and round the value to the nearest 1 km. The greatest weight is given to slip inversion results, followed by hypocentral depths constrained by local stations. If local depth estimates are unavailable, then the depth range is estimated as ± 4 %, from the best fit of the depth sensitivity for waveform moment tensor inversion from the Saint Louis University Earthquake Center (*23*). We find that more than half of induced earthquakes appear to be shallower than 5 km, whereas all the tectonic earthquakes in the central United States are deeper than 5 km (Fig. 4). Tables S2 to S4 summarize source parameters of analyzed earthquakes, including moment magnitudes, depths, corner frequency estimates, and stress drop estimates.

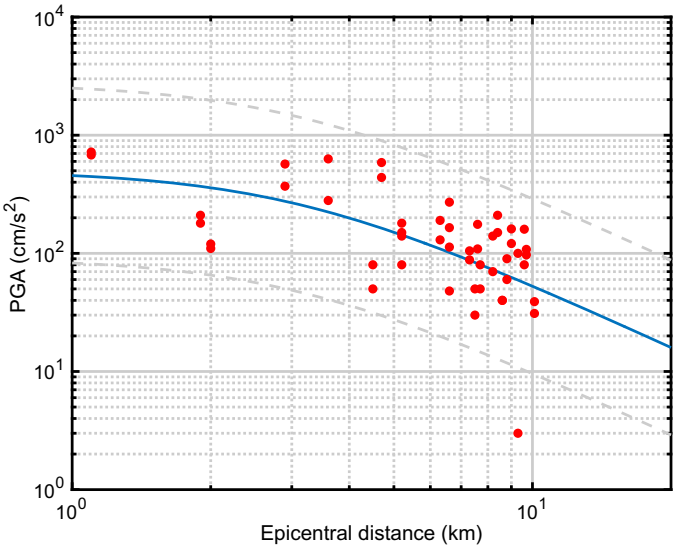

Fig. 1. Peak ground acceleration (PGA) measured from the geometric mean of horizontal components recorded by U.S. Geological Survey strong motion instruments for seven recent M_w 4 to 4.5 earthquakes in Oklahoma, Kansas, and Texas (red dots, table S1). The predicted ground motions for an M_w 4.5 earthquake (blue solid line) and its 95% confidence interval (gray dashed lines) are calculated using the Ground Motion Prediction Equation (GMPE) from Atkinson (*9*).

Figure 3 shows that the population of deeper induced earthquakes has a median stress drop of 13.1 MPa. These induced earthquakes with M_w of 3.3 to 5.8 have a comparable median stress drop to tectonic earthquakes in the central United States at comparable focal depths. Our results support the notion that induced earthquakes release tectonic stress in the same manner as tectonic earthquakes and should be expected to produce similar levels of ground motions (*1*).

In contrast to earthquakes in the central United States, the eight tectonic earthquakes in the eastern North America show stress drops between 1.1 and 111 MPa with a higher median of 29 MPa. Most eastern earthquakes occur on reverse faults, whereas most central U.S. induced and tectonic earthquakes occur on strike-slip faults. The difference in faulting styles is an additional factor that can influence stress drop and hence ground motion. Reverse-faulting regimes are expected to have a vertically oriented minimum principal stress, such that shear stress across the fault is expected to be higher than for normal-faulting and strike-slip regimes. It leads to potentially larger stress drops if the stress drop is proportional to the crustal stress. To quantify the expected effects of faulting style and earthquake depth, we apply a relationship of principal stresses, pore pressure, and frictional coefficient, assuming

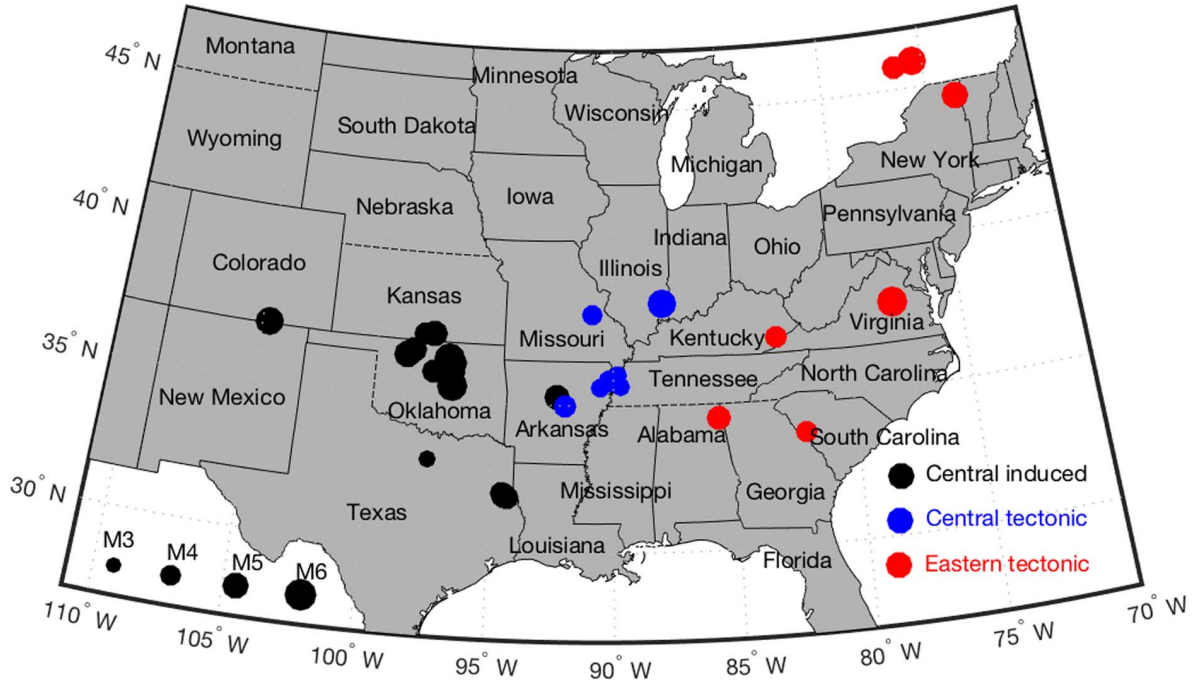

Fig. 2. Locations of analyzed earthquakes.

Downloaded from http://advances.sciencemag.org/ on September 24, 2020

that the ratio of the maximum to the minimum effective stress is determined by stresses on optimally oriented preexisting faults (*24*)

$$\frac{\sigma_1 - P}{\sigma_3 - P} = [(1 + \mu^2)^{\frac{1}{2}} + \mu]^2 \quad (1)$$

where σ_1 is the maximum principal stress, σ_3 is the minimum principal stress, P is the pore pressure, and μ is the frictional coefficient. We derive the ratio of the maximum to the minimum effective stress, assuming a frictional coefficient of 0.6. Most rocks show a friction coefficient of 0.6 at an effective normal stress appropriate for the crust (*25*). As the crustal shear strength $S = (\sigma_1 - \sigma_3)/2$, we show that for reverse-faulting and normal-faulting earthquakes

$$S_{\text{reverse}} = 1.06(\sigma_v - P) \quad (2)$$

$$S_{\text{normal}} = 0.34(\sigma_v - P) \quad (3)$$

where σ_v is the vertical stress. The crustal shear strengths of strike-slip faults should lie between these two. For simplicity, we use their average

$$S_{ss} = 0.7(\sigma_v - P) \quad (4)$$

Assuming that intraplate faults are critically stressed with hydrostatic pore pressure (*26*) yields a gradient of 17 MPa/km for the effective normal stress ($\sigma_v - P$). If the fault has an available shear stress of $\Delta\tau_{\text{total}}$ such that the shear stress decreases from the crustal shear strength to 0, we find that stress drops of most earthquakes fall between 5% $\Delta\tau_{\text{total}}$ and 50% $\Delta\tau_{\text{total}}$ with an average of ~15 to 20% $\Delta\tau_{\text{total}}$ for both strike-slip and reverse-faulting regimes (Fig. 4). Note that there are only two normal-faulting earthquakes in the data set: the 2011 M_w 5.3 Trinidad earthquake and the 2014 M_w 4.3 Milan foreshock. Induced earthquakes also have a wider range of stress drop than tectonic earthquakes. The 2011 M_w 5.0 Prague foreshock and the 2016 M_w 5.8 Pawnee mainshock show nearly total stress drops (Fig. 4), indicating that their rupture processes may have released all available shear stress on the rupture surface.

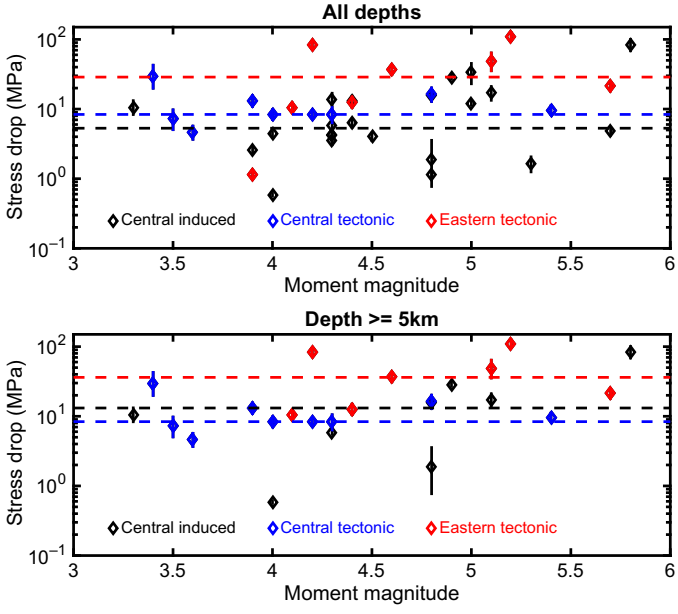

Fig. 3. Stress drop estimates of induced and tectonic earthquakes at all depths (top) and deeper than 5 km (bottom) as a function of moment magnitude. Dashed lines show the median stress drop for each group. Error bars denote 95% confidence level based on bootstrap analysis.

DISCUSSION

Depth dependence

We show that the median stress drop of induced earthquakes increases by a factor of >2 when earthquakes deeper than 5 km are considered. This suggests a possible correlation between stress drop and depth, which is otherwise obscured by the wide range of stress drop estimates for strike-slip earthquakes (Fig. 4). This depth dependence is also consistent with the population of six reverse-faulting earthquakes in the eastern North America. The 2011 M_w 3.9 Virginia earthquake with the smallest stress drop is the shallowest, whereas the 2010 M_w 5.2 Quebec earthquake with the highest stress drop is the deepest. Because our stress drops are calculated using a constant *S*-wave velocity,

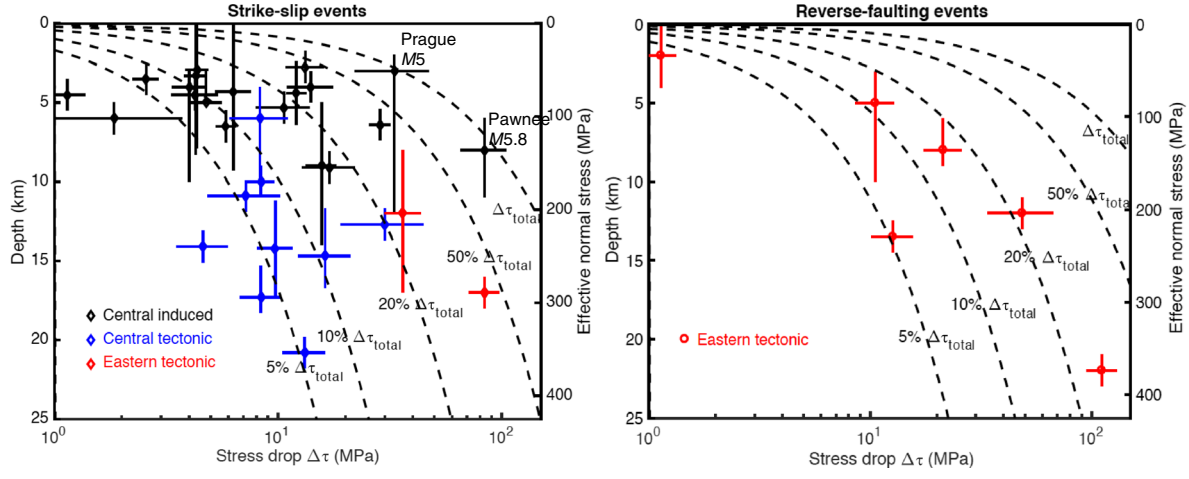

Fig. 4. Stress drop estimates as a function of earthquake depth for strike-slip events and reverse-faulting events. Horizontal error bars show bootstrapped 95% confidence level for stress drop. Vertical error bars show the possible range of earthquake depths. The depth gradient of the effective normal stress is 17 MPa/km. Dashed lines indicate fractional stress drops. The top right of the left panel shows the two events with nearly total stress drops: the 2011 M_w 5.0 Prague foreshock and the 2016 M_w 5.8 Pawnee mainshock.

Downloaded from http://advances.sciencemag.org/ on September 24, 2020

this depth dependence may be compensated by an increase of the local *S*-wave velocity with depth (*27*); however, the observed stress drop variation with depth would require an unrealistically rapid increase in *S*-wave velocity with depth. For example, a stress drop of 10 MPa at 5 km and an average stress drop gradient of 10% $\Delta\tau_{total}$ would imply a velocity increase from a crustal value at 5 km to a mantle value at 10 km, which is highly improbable in eastern North America (*28*). This depth dependence of stress drops is more likely caused by the expected increase of the effective normal stress. We note that in contrast to our results, Allman and Shearer (*29*) did not find a clear depth dependence in their study of global seismicity; however, they estimated stress drop using a different approach, and their results are collated over the full range of tectonic regimes.

Comparison with other stress drop studies

Our stress drop estimates are generally consistent with stress drop estimates from finite fault slip models. We find that the 2011 M_w 5.7 Prague, the 2008 M_w 5.4 Mount Carmel, and the 2011 M_w 5.7 Virginia earthquakes have stress drops of 4.8, 9.7, and 21 MPa, respectively. Finite fault models for the same earthquakes lead to stress drops of 1.6 MPa (9 MPa for the largest slip patch) (*30*), 10 MPa (*31*), and 15 to 25 MPa (*32*), respectively. Stress drop of the Virginia earthquake could be even higher (for example, 30 to 75 MPa), as suggested by other spectral ratio and waveform modeling studies (*33*–*35*). We note that the circular crack model assumes a constant stress drop, whereas finite-source images of rupture commonly reveal a more complex rupture process. Departures from the constant stress drop model require locally higher-than-average stress drop within the faulted area. For example, the 2011 M_w 5.7 Virginia earthquake is observed to have two large subevents (*32*, *35*). Some earthquakes in our analysis, for example, the M_w 4.8 Guy-Greenbrier earthquake and the M_w 5.3 Trinidad earthquake, may be better modeled using a double-corner-frequency model (*36*, *37*). The uncertainty in stress drop estimates for these earthquakes may be reduced by selecting a source model based on the shape of the observed spectral ratio or the *P*-to-*S* corner frequency ratios (*38*), but a single source model is assumed here to facilitate comparison between induced and tectonic earthquakes.

The observed stress drops also lead to ground motions with comparable intensity. Among the three Timpson earthquakes in 2013, the January 25 event with a high stress drop of 13.3 MPa and a shallow depth of 2.75 km also gave rise to the highest reported shaking intensity. The average stress parameters of eight tectonic earthquakes in eastern North America show a range of 18 to 25 MPa (*39*), comparable with the median stress drop of eastern tectonic earthquakes in our analysis. Our results also agree with stress drop estimates in other spectral ratio studies. Viegas *et al.* (*40*) gave a similar *S*-wave corner frequency estimate for the 2002 M_w 5.1 Au Sable Forks earthquake (1.7 Hz versus 1.6 Hz), although they used a Boatwright spectral model instead of a Brune spectral model. In the study of Boyd *et al.* (*41*), 9 of 12 events common to our studies show corner frequencies within a factor of 1.5 (table S5). Note that the uncertainties in the corner frequency estimates reported by Boyd *et al.* (*41*) are usually not within the uncertainties in our estimates. We both calculate uncertainties by quantifying how well the model fits the observed spectral ratio; however, the actual uncertainties in these estimates are likely to be larger because the corner frequency difference may result from the choices of eGf events, stations, and *S*-wave window lengths, whereas the stress drop values are also affected by seismic moments, *S*-wave velocities, and the spectral source model. Stress drop estimates from the spectral ratio method are often higher than those from the constant attenuation approach used to interpret individual spectra due to a more effective removal of propagation path effects (*42*), so a direct comparison between stress drop estimates calculated from these two methods may not be feasible.

Relevance to ground motion prediction

GMPEs are commonly used to quantify the level of ground shaking for a given earthquake. Because GMPEs have been developed primarily using recordings of tectonic earthquakes, the question of whether they can be applied, without modification, for predicting ground motions from induced earthquakes remains. The comparable stress drops of induced and tectonic earthquakes we find in the central United States suggest that their ground motions can be described by the same set of equations, provided that similar magnitudes, distances, and depths are considered (*9*, *43*–*45*). Although ground motions of earthquakes in the central and eastern United States are usually analyzed together because of a lack of data, our results support a separation of these two groups of tectonic earthquakes in the future development of GMPEs, which could be achieved by specifying the faulting style. The higher stress drops of eastern tectonic earthquakes also help explain why induced earthquakes show lower "Did You Feel It?" intensities than the predicted intensities based on equations derived from ground motions of central and eastern tectonic earthquakes in aggregate. We note that eastern tectonic earthquakes comprise more than half of the tectonic earthquakes (6 of 10) in the "Did You Feel It?" intensity comparison of induced and tectonic earthquakes (*4*). We also find that stress drops of three of the four central tectonic earthquakes analyzed in the "Did You Feel It?" study, including the 2008 M_w 5.4 Mount Carmel (9.7 MPa), the 2008 M_w 4.8 Mount Carmel (16.3 MPa), and the 2005 M_w 4.2 Arkansas (8.4 MPa) earthquakes, are higher than or equal to the median stress drop of central tectonic earthquakes in our analysis.

The depth dependence of our stress drop estimates suggests that we should expect more intense ground motion from deeper earthquakes. McGarr (*46*) characterized the expected depth dependence using the ground acceleration parameter, ρRa, where ρ is the density, R is the hypocentral distance, and a is the peak acceleration. The ground acceleration parameter is independent of earthquake size but increases with depth with a gradient of 3.1 MPa/km for normal faulting and 8.8 MPa/km for reverse faulting. Most of the earthquakes in our analysis are strike-slip events, which show an average depth gradient of ~20% $\Delta\tau_{total}$ or ~3.4 MPa/km that lies between these limits. On the other hand, shallower earthquakes tend to produce larger ground motions at near-fault distances (*9*), and it is important to consider both the effects of depth-dependent stress drops and propagation effects for predicting ground motions of induced earthquakes.

CONCLUSIONS

We measure stress drops of induced and tectonic earthquakes with M_w of 3.3 to 5.8 using eGf spectral ratios. We find that induced earthquakes have a comparable median stress drop to tectonic earthquakes in the central United States. We also find that tectonic earthquakes in the eastern North America exhibit a much higher median stress drop, which is consistent with independent source parameter estimates and may be attributable to greater driving stress due to a combination of reverse faulting and greater depth. Our results support similar ground motions from induced and shallow tectonic earthquakes, given the same depth and tectonic setting. This is consistent with the hypothesis that induced

Downloaded from http://advances.sciencemag.org/ on September 24, 2020

earthquakes are triggered by fluid injection but driven by tectonic stresses. We conclude that GMPEs developed for tectonic earthquakes in the central United States can be applied to induced earthquakes.

MATERIALS AND METHODS

The spectral ratio approach assumes that two colocated earthquakes share the same propagation path and site effects. The ideal spectral ratio of these two earthquakes shows two plateaus that correspond to frequencies lower than the corner frequency of the target earthquake and higher than the corner frequency of the smaller eGf event. The second plateau may be absent in the observed spectral ratio because of the limited bandwidth at high frequency. Using the Brune spectral model (*17*), the ideal spectral ratio is described as

$$\frac{u_1(f)}{u_2(f)} = \frac{M_{01}}{M_{02}} \left(\frac{1 + (\frac{f}{f_{c2}})^2}{1 + (\frac{f}{f_{c1}})^2} \right) \quad (5)$$

where $u_1(f)$ is the displacement spectrum of the master event, $u_2(f)$ is the displacement spectrum of the eGf, M_{01} is the seismic moment of the master event, f_{c1} is the corner frequency of the master event, M_{02} is the seismic moment of the eGf, and f_{c2} is the corner frequency of the eGf. Note that $u_1(f)$ and $u_2(f)$ can also be the velocity or acceleration spectrum.

We used seismic data recorded by broadband stations (table S6) to calculate spectral ratios. We chose frequency bands and stations that have good signal-to-noise ratios, and thus, the frequency bands and distance range of stations vary for events with different magnitudes. The frequency bands for spectral analysis are shown in figs. S1 to S3. The stations are typically within 200 to 300 km for an *M*5 earthquake and within 100 to 200 km for an *M*4 earthquake. Depending on the regions, the stations can have a sampling rate of 20, 40, 50, 100, and 200 sps. Figures S4 and S5 show the east-component velocity seismograms for the 2016 M_w 5.1 Fairview earthquake and its eGf at two stations. In practice, small differences in earthquake locations may cause imperfect separation of source and propagation path effects, leading to unstable calculation of spectral ratios. We used multiple windows following direct *S* waves to stabilize the results (*16*). We used five windows overlapped by half the duration of the window length, as shown by the colored lines under velocity seismograms in figs. S4 and S5. For each window, we sampled the spectrum at equal intervals of 0.025 in log frequency and smoothed it with a running average over four samples. We then stacked the spectral ratios over five windows for each station. The final *S*-wave spectral ratio for each master-eGf pair was obtained from stacking over all the stations and averaging from both east and north components. Similar to Huang *et al.* (*6*), we used the trust region reflective optimization in MATLAB (lsqnonlin@MATLAB) to model the spectral ratio. An upper bound of 80% of the Nyquist frequency is given to ensure the resolution of the corner frequency estimate.

We found that the choice of the window length can significantly affect the corner frequency estimate. To ensure that the observed spectral ratio is well described by the Brune spectral model, we calculated spectral ratios using various window lengths and chose the window length that minimized the misfits between the stacked spectral ratio and the Brune spectral model. Figure S6 shows that a window length of 4 s leads to the smallest misfit for the 2016 M_w 5.1 Fairview earthquake and hence the best corner frequency estimate. The corner frequency value tends to stabilize as the window length increases. We also found that larger earthquakes are more likely to require a longer window length. The best-fit spectral ratio of the 2011 M_w 5.7 Prague earthquake is derived from 14-s-long windows.

We applied a bootstrap analysis to calculate the range of corner frequency estimates at the 95% confidence level. The residuals between the best-fit model and the stacked spectral ratios were resampled at each frequency interval and then added to the stacked spectral ratios to create synthetic spectral ratios, which resulted in a new corner frequency estimate each time. By carrying out this procedure 1000 times, we obtained 1000 corner frequency estimates, which usually appear as a Gaussian distribution if the best-fit corner frequency is well constrained (fig. S7).

We calculate stress drop from seismic moment M_0 and corner frequency f_c, assuming a circular crack model (*19*) and Brune's source model (*17*)

$$\Delta\tau = \frac{7}{16}\frac{M_0}{r^3} \quad (6)$$

$$r = \frac{0.372 v_s}{f_c} \quad (7)$$

where r is the source radius and v_s is the *S*-wave velocity (3.3 km/s). The choice of the Brune model over alternatives (*20*, *21*) has a much larger effect on stress drop than variations in *S*-wave velocity. For example, changing from 3.3 to 4 km/s decreases the model stress drop by less than a factor of 2. Alternatively, using $r = \frac{0.21 v_s}{f_c}$ from Madariaga's source parameter (*21*) increases the stress drop by a factor of ~5.

SUPPLEMENTARY MATERIALS

Supplementary material for this article is available at http://advances.sciencemag.org/cgi/content/full/3/8/e1700772/DC1

fig. S1. Observed *S*-wave spectral ratios of potentially induced earthquakes to their eGfs (colored solid lines) and modeled spectral ratios (gray dashed lines).
fig. S2. Observed *S*-wave spectral ratios of tectonic earthquakes in the central United States to their eGfs (colored solid lines) and modeled spectral ratios (gray dashed lines).
fig. S3. Observed *S*-wave spectral ratios of tectonic earthquakes in eastern North America to their eGfs (colored solid lines) and modeled spectral ratios (gray dashed lines).
fig. S4. East-component velocity seismograms and spectra recorded at station KAN06 for the 2016 M_w 5.1 Fairview earthquake (event #1) and its eGf (event #3).
fig. S5. East-component velocity seismograms and spectra recorded at station OK033 for the 2016 M_w 5.1 Fairview earthquake (event #1) and its eGf (event #3).
fig. S6. The misfits between the Brune spectral model and the stacked spectral ratios, and the corner frequency estimates derived from different window lengths for the 2016 M_w 5.1 Fairview earthquake.
fig. S7. Histograms of the corner frequency distribution from the bootstrap analysis for four Oklahoma earthquakes.
table S1. Near-source peak ground accelerations of potentially induced earthquakes in the central United States.
table S2. Source parameters of potentially induced earthquakes in the central United States.
table S3. Source parameters of tectonic earthquakes in the central United States.
table S4. Source parameters of tectonic earthquakes in eastern North America.
table S5. Comparison of source parameters between the study of Boyd *et al.* (*41*) and this study.
table S6. Networks and number of stations used in this study.
References (*47*–*59*)

REFERENCES AND NOTES

1. W. L. Ellsworth, Injection-induced earthquakes. *Science* **341**, 1225942 (2013).
2. T. C. Hanks, *b* values and $\omega^{-\gamma}$ seismic source models: Implications for tectonic stress variations along active crustal fault zones and the estimation of high-frequency strong ground motion. *J. Geophys. Res.* **84**, 2235–2242 (1979).

Downloaded from http://advances.sciencemag.org/ on September 24, 2020

3. D. M. Boore, Stochastic simulation of high-frequency ground motions based on seismological models of the radiated spectra. *Bull. Seismol. Soc. Am.* **73**, 1865–1894 (1983).
4. S. E. Hough, Shaking from injection-induced earthquakes in the central and eastern United States. *Bull. Seismol. Soc. Am.* **104**, 2619–2626 (2014).
5. S. E. Hough, Shaking intensity from injection-induced versus tectonic earthquakes in the central-eastern United States. *Leading Edge* **34**, 690–697 (2015).
6. Y. Huang, G. C. Beroza, W. L. Ellsworth, Stress drop estimates of potentially induced earthquakes in the Guy-Greenbrier sequence. *J. Geophys. Res.* **121**, 6597–6607 (2016).
7. H. Zhang, D. W. Eaton, G. Li, Y. Liu, R. M. Harrington, Discriminating induced seismicity from natural earthquakes using moment tensors and source spectra. *J. Geophys. Res.* **121**, 972–993 (2016).
8. F. Clerc, R. M. Harrington, Y. Liu, Y. J. Gu, Stress drop estimates and hypocenter relocations of induced seismicity near Crooked Lake, Alberta. *Geophys. Res. Lett.* **43**, 6942–6951 (2016).
9. G. M. Atkinson, Ground-motion prediction equation for small-to-moderate events at short hypocentral distances, with application to induced-seismicity hazards. *Bull. Seismol. Soc. Am.* **105**, 981–992 (2015).
10. H. Berckhemer, Die Ausdehnung der Bruchfläche im Erdbebenherd und ihr Einfluss auf das seismische Wellenspektrum. *Gerlands Beitr. Geophys.* **71**, 5–26 (1962).
11. K. Aki, Scaling law of seismic spectrum. *J. Geophys. Res.* **72**, 1217–1231 (1967).
12. C. S. Mueller, Source pulse enhancement by deconvolution of an empirical Green's function. *Geophys. Res. Lett.* **12**, 33–36 (1985).
13. S. E. Hough, Empirical Green's function analysis: Taking the next step. *J. Geophys. Res.* **102**, 5369–5384 (1997).
14. A. S. Baltay, T. C. Hanks, G. C. Beroza, Stable stress drop measurements and their variability: Implications for ground motion prediction. *Bull. Seismol. Soc. Am.* **103**, 211–222 (2013).
15. R. E. Abercrombie, Investigating uncertainties in empirical Green's function analysis of earthquake source parameters. *J. Geophys. Res. Solid Earth* **120**, 4263–4377 (2015).
16. K. Imanishi, W. L. Ellsworth, Source scaling relationships of microearthquakes at Parkfield, CA, determined using the SAFOD pilot hole seismic array, in *Earthquakes: Radiated Energy and the Physics of Faulting*, R. Abercrombie, A. Mcgarr, G. D. Di Toro, H. Kanamori, Eds. (AGU, 2006).
17. J. Brune, Tectonic stress and the spectra of seismic shear waves from earthquakes. *J. Geophys. Res.* **75**, 4997–5009 (1970).
18. J. D. Eshelby, The determination of the elastic field of an ellipsoidal inclusion, and related problems. *Proc. R. Soc. London* **241**, 376–396 (1957).
19. J. Boatwright, A spectral theory for circular seismic sources: Simple estimates of source dimension, dynamic stress drop and radiated seismic energy. *Bull. Seismol. Soc. Am.* **70**, 1–28 (1980).
20. T. Sato, T. Hirasawa, Body wave spectra from propagating shear cracks. *J. Phys. Earth* **21**, 415–431 (1974).
21. R. Madariaga, Dynamics of an expanding circular fault. *Bull. Seismol. Soc. Am.* **66**, 639–666 (1976).
22. Y. Kaneko, P. M. Shearer, Variability of seismic source spectra, estimated stress drop, and radiated energy, derived from cohesive-zone models of symmetrical and asymmetrical circular and elliptical ruptures. *J. Geophys. Res.* **120**, 1053–1079 (2015).
23. Department of Earth and Atmospheric Sciences, Saint Louis University, "North America Moment Tensor," www.eas.slu.edu/eqc/eqc_mt/MECH.NA/.
24. D. Moos, M. D. Zoback, Utilization of observations of well bore failure to constrain the orientation and magnitude of crustal stresses: Application to continental, Deep Sea Drilling Project, and Ocean Drilling Program boreholes. *J. Geophys. Res.* **95**, 9305–9325 (1990).
25. J. Byerlee, Friction of rocks. *Pure Appl. Geophys.* **116**, 615–626 (1978).
26. J. Townend, M. D. Zoback, How faulting keeps the crust strong. *Geology* **28**, 399–402 (2000).
27. B. P. Allmann, P. M. Shearer, Spatial and temporal stress drop variations in small earthquakes near Parkfield, California. *J. Geophys. Res.* **112**, B04305 (2007).
28. L. C. Pakiser, W. D. Mooney, *Geophysical Framework of the Continental United States* (Geological Society of America, 1989), vol. 172.
29. B. P. Allman, P. M. Shearer, Global variations of stress drop for moderate to large earthquakes. *J. Geophys. Res.* **114**, B01310 (2009).
30. X. Sun, S. Hartzell, Finite-fault slip model of the 2011 M_w 5.6 Prague, Oklahoma earthquake from regional waveforms. *Geophys. Res. Lett.* **41**, 4207–4213 (2014).
31. S. Hartzell, C. Mendoza, Source and site response study of the 2008 Mount Carmel, Illinois, earthquake. *Bull. Seismol. Soc. Am.* **101**, 951–963 (2011).
32. S. Hartzell, C. Mendoza, Y. Zeng, Rupture model of the 2011 Mineral, Virginia, earthquake from teleseismic and regional waveforms. *Geophys. Res. Lett.* **40**, 5665–5670 (2013).
33. C. H. Cramer, J. Kutliroff, D. Dangkua, paper presented at the 2011 Annual Meeting of American Geophysical Union, San Francisco, CA, 5 to 9 December 2011.
34. W. L. Ellsworth, K. Imanishi, J. H. Luetgert, J. Kruger, J. Hamilton, paper presented at the 2011 Annual Meeting of American Geophysical Union, San Francisco, CA, 5 to 9 December 2011.
35. M. C. Chapman, On the rupture process of the August 23, 2011 Virginia earthquake. *Bull. Seismol. Soc. Am.* **103**, 613–628 (2013).
36. M. A. Denolle, P. M. Shearer, New perspectives on self-similarity for shallow thrust earthquakes. *J. Geophys. Res. Solid Earth* **121**, 6533–6565 (2016).
37. T. Uchide, K. Imanishi, Small earthquakes deviate from the omega-square model as revealed by multiple spectral ratio analysis. *Bull. Seismol. Soc. Am.* **106**, 1357–1363 (2016).
38. R. E. Abercrombie, S. Bannister, J. Ristau, D. Doser, Variability of earthquake stress drop in a subduction setting, the Hikurangi Margin, New Zealand. *Geophys. J. Int.* **208**, 306–320 (2017).
39. D. M. Boore, K. W. Campbell, G. M. Atkinson, Determination of stress parameters for eight well-recorded earthquakes in eastern North America. *Bull. Seismol. Soc. Am.* **100**, 1632–1645 (2010).
40. G. Viegas, R. E. Abercrombie, W.-Y. Kim, The 2002 M5 Au Sable Forks, NY, earthquake sequence: Source scaling relationships and energy budget. *J. Geophys. Res.* **115**, B07310 (2010).
41. O. S. Boyd, D. E. McNamara, S. Hartzell, G. Choy, *Bull. Seismol. Soc. Am.* **107**, (2017).
42. S. Ide, G. C. Beroza, S. G. Prejean, W. L. Ellsworth, Apparent break in earthquake scaling due to path and site effects on deep borehole recordings. *J. Geophys. Res.* **108**, 2271 (2003).
43. J. Douglas, B. Edwards, V. Convertito, N. Sharma, A. Tramelli, D. Kraaijpoel, B. Mena Cabrera, N. Maercklin, C. Troise, Predicting ground motion from induced earthquakes in geothermal areas. *Bull. Seismol. Soc. Am.* **103**, 1875–1897 (2013).
44. J. J. Bommer, B. Dost, B. Edwards, P. J. Stafford, J. van Elk, D. Doornhof, M. Ntinalexis, Developing an application-specific ground-motion model for induced seismicity. *Bull. Seismol. Soc. Am.* **106**, 158–173 (2016).
45. A. Gupta, J. W. Baker, W. L. Ellsworth, Assessing ground-motion amplitudes and attenuation for small-to-moderate induced and tectonic earthquakes in the central and eastern United States. *Seismol. Res. Lett.* **88**, 10.1785/0220160199 (2017).
46. A. McGarr, Scaling of ground motion parameters, state of stress, and focal depth. *J. Geophys. Res.* **89**, 6969–6979 (1984).
47. S. Horton, Disposal of hydrofracking waste fluid by injection into subsurface aquifers triggers earthquake swarm in Central Arkansas with potential for damaging earthquake. *Seismol. Res. Lett.* **83**, 250–260 (2012).
48. W. D. Barnhart, H. M. Benz, G. P. Hayes, J. L. Rubinstein, E. Bergman, Seismological and geodetic constraints on the 2011 M_w5.3 Trinidad, Colorado earthquake and induced deformation in the Raton Basin. *J. Geophys. Res. Solid Earth* **119**, 7923–7933 (2014).
49. C. Frohlich, W. Ellsworth, W. A. Brown, M. Brunt, J. Luetgert, T. MacDonald, S. Walter, The 17 May 2012 *M*4.8 earthquake near Timpson, East Texas: An event possibly triggered by fluid injection. *J. Geophys. Res. Solid Earth* **119**, 581–593 (2014).
50. M. J. Hornbach, H. R. DeShon, W. L. Ellsworth, B. W. Stump, C. Hayward, C. Frohlich, H. R. Oldham, J. E. Olson, M. B. Magnani, C. Brokaw, J. H. Luetgert, Causal factors for seismicity near Azle, Texas. *Nat. Commun.* **6**, 6728 (2015).
51. G. L. Choy, J. L. Rubinstein, W. L. Yeck, D. E. McNamara, C. S. Mueller, O. S. Boyd, A rare moderate-sized (M_w 4.9) earthquake in Kansas: Rupture process of the Milan, Kansas, earthquake of 12 November 2014 and its relationship to fluid injection. *Seismol. Res. Lett.* **87**, 1433–1441 (2016).
52. D. E. McNamara, G. P. Hayes, H. M. Benz, R. A. Williams, N. D. McMahon, R. C. Aster, A. Holland, T. Sickbert, R. Herrmann, R. Briggs, G. Smoczyk, E. Bergman, P. Earle, Reactivated faulting near Cushing, Oklahoma: Increased potential for a triggered earthquake in an area of United States strategic infrastructure. *Geophys. Res. Lett.* **42**, 8328–8332 (2015).
53. Earthquake catalogs are available at U.S. Geological Survey National Earthquake Information Center, http://earthquake.usgs.gov/earthquakes/.
54. W. L. Yeck, M. Weingarten, H. M. Benz, D. E. McNamara, E. A. Bergman, R. B. Herrmann, J. L. Rubinstein, P. S. Earle, Far-field pressurization likely caused one of the largest injection induced earthquakes by reactivating a large preexisting basement fault structure. *Geophys. Res. Lett.* **43**, 10198–10207 (2016).
55. R. B. Herrmann, M. Withers, H. Benz, The April 18, 2008 Illinois earthquake: An ANSS monitoring success. *Seismol. Res. Lett.* **79**, 830–843 (2008).
56. H. Yang, L. Zhu, R. Chu, Fault-plane determination of the 18 April 2008 Mount Carmel, Illinois, Earthquake by detecting and relocating aftershocks. *Bull. Seismol. Soc. Am.* **99**, 3413–3420 (2009).
57. M. W. Hamburger, K. Shoemaker, S. Horton, H. DeShon, M. Withers, G. L. Pavlis, E. Sherrill, Aftershocks of the 2008 Mt. Carmel, Illinois, Earthquake: Evidence for conjugate faulting near the termination of the Wabash Valley Fault System. *Seismol. Res. Lett.* **82**, 735–747 (2011).

Downloaded from http://advances.sciencemag.org/ on September 24, 2020

58. S. Ma, G. M. Atkinson, Focal depths for small to moderate earthquakes ($m_N \geq 2.8$) in Western Quebec, Southern Ontario, and Northern New York. *Bull. Seismol. Soc. Am.* **96**, 609–623 (2006).
59. Earthquake catalogs are available at Canadian Earthquake Database, www.earthquakescanada.nrcan.gc.ca/index-en.php.

Acknowledgments: We thank R. Abercrombie and an anonymous reviewer for the helpful comments. **Funding:** This work was supported by the Stanford Center for Induced and Triggered Seismicity. **Author contributions:** Y.H. carried out the corner frequency and stress drop analysis, and W.L.E. compiled peak ground accelerations of induced earthquakes. Y.H., W.L.E., and G.C.B. contributed to the interpretation of the results and wrote the manuscript. **Competing interests:** G.C.B. and W.L.E. are codirectors of the Stanford Center for Induced and Triggered Seismicity. The authors declare that they have no other competing interests. **Data and materials availability:** Seismic data used in this study are available at IRISDMC (IRIS Data Management Center). All data needed to evaluate the conclusions in the paper are present in the paper and/or the Supplementary Materials. Additional data related to this paper may be requested from the authors.

Submitted 9 March 2017
Accepted 28 June 2017
Published 2 August 2017
10.1126/sciadv.1700772

Citation: Y. Huang, W. L. Ellsworth, G. C. Beroza, Stress drops of induced and tectonic earthquakes in the central United States are indistinguishable. *Sci. Adv.* **3**, e1700772 (2017).

Downloaded from http://advances.sciencemag.org/ on September 24, 2020

Science Advances

Stress drops of induced and tectonic earthquakes in the central United States are indistinguishable

Yihe Huang, William L. Ellsworth and Gregory C. Beroza

Sci Adv **3** (8), e1700772.
DOI: 10.1126/sciadv.1700772

ARTICLE TOOLS http://advances.sciencemag.org/content/3/8/e1700772

SUPPLEMENTARY MATERIALS http://advances.sciencemag.org/content/suppl/2017/07/28/3.8.e1700772.DC1

REFERENCES This article cites 50 articles, 17 of which you can access for free
http://advances.sciencemag.org/content/3/8/e1700772#BIBL

PERMISSIONS http://www.sciencemag.org/help/reprints-and-permissions

Use of this article is subject to the Terms of Service

Science Advances (ISSN 2375-2548) is published by the American Association for the Advancement of Science, 1200 New York Avenue NW, Washington, DC 20005. The title *Science Advances* is a registered trademark of AAAS.

Copyright © 2017 The Authors, some rights reserved; exclusive licensee American Association for the Advancement of Science. No claim to original U.S. Government Works. Distributed under a Creative Commons Attribution NonCommercial License 4.0 (CC BY-NC).

Downloaded from http://advances.sciencemag.org/ on September 24, 2020